J. Fluid Mech. (2004), *vol.* 527, *pp.* 27–55.
DOI: 10.1017/S0022112004002575 Printed in the United Kingdom

Displacement and mixing ventilation driven by opposing wind and buoyancy

By G. R. HUNT[1] AND P. F. LINDEN[2]

[1]Department of Civil and Environmental Engineering, Imperial College London, London SW7 2AZ, UK

[2]Department of Mechanical and Aerospace Engineering, University of California, San Diego, 9500 Gilman Drive, La Jolla, CA 92093-0411, USA

(Received 10 August 2001 and in revised form 17 September 2004)

The effect of an opposing wind on the stratification and flow produced by a buoyant plume rising from a heat source on the floor of a ventilated enclosure is investigated. Ventilation openings located at high level on the windward side of the enclosure and at low level on the leeward side allow a wind-driven flow from high to low level, opposite to the buoyancy-driven flow. One of two stable steady flow regimes is established depending on a dimensionless parameter F that characterizes the relative magnitudes of the wind-driven and buoyancy-driven velocities within the enclosure, and on the time history of the flow. A third, unstable steady flow solution is identified. For small opposing winds (small F) a steady, two-layer stratification and *displacement ventilation* is established. Exterior fluid enters through the lower leeward openings and buoyant interior fluid leaves through the upper windward openings. As the wind speed increases, the opposing wind may cause a reversal in the flow direction. In this case, cool exterior fluid enters through the high windward openings and mixes the interior fluid, which exits through the leeward openings. There are now two possibilities. If the rate of heat input by the source exceeds the rate of heat loss through the leeward openings, the temperature of the interior increases and this flow reversal is only maintained temporarily. The buoyancy force increases with time, the flow reverts to its original direction, and steady two-layer displacement ventilation is re-established and maintained. In this regime, the increase in wind speed increases the depth and temperature of the warm upper layer, and reduces the ventilation flow rate. If, on the other hand, the heat loss exceeds the heat input, the interior cools and the buoyancy-driven flow decreases. The reversed flow is maintained, the stratification is destroyed and *mixing ventilation* occurs. Further increases in wind speed increase the ventilation rate and decrease the interior temperature.

The transitions between the two ventilation flow patterns exhibit hysteresis. The change from displacement ventilation to mixing ventilation occurs at a higher F than the transition from mixing to displacement. Further, we find that the transition from mixing to displacement ventilation occurs at a fixed value of F, whereas the transition from displacement to mixing flow is dependent on the details of the time history of the flow and the geometry of the openings, and is not determined solely by the value of F.

Theoretical models that predict the steady stratification profiles and flow rates for the displacement and mixing ventilation, and the transitions between them, are presented and compared with measurements from laboratory experiments. The transition between these ventilation patterns completely changes the internal environment, and we discuss some of the implications for the natural ventilation of buildings.

1. Introduction

Natural ventilation harnesses the wind, and also the buoyancy forces associated with temperature differences between the interior and exterior environments, to drive air flow through a building. High Reynolds number flow around an isolated building creates positive pressures on the windward side and negative pressures in the lee. By suitably locating openings that connect the interior and exterior environments this wind-induced pressure difference Δ may be harnessed to drive a ventilation flow through the building.

Depending on the location of the openings, the buoyancy forces (or stack effect) may assist (Hunt & Linden 1999, 2001) or oppose the wind-driven flow (Hunt & Linden 2000; Li & Delsante 2001). Furthermore, the opening location strongly affects the rate of air exchange and stratification that develops in the interior of the building. For example, if openings are made such that cool air enters at high level, the incoming air is tempered as it mixes with the warmer internal air: rates of air exchange are low and the space cools relatively slowly. Vertical temperature gradients are weak and temperatures are fairly uniform throughout the space. If, on the other hand, cool air enters at low levels and warm air is displaced from the space through openings at high level, a stable stratification typically develops in the interior. Warm air collects in a zone near the ceiling and cooling is achieved as the lower zone is flushed with cool ambient air – rates of air exchange and cooling are significantly higher than for mixing flows. These flows are referred to as *mixing ventilation* and *displacement ventilation*, respectively. For a given internal heat flux, since the temperature of the air leaving the building is lower, the ventilation flow rate required to maintain a steady state is larger for mixing ventilation than for displacement ventilation.

In cool and temperate climates, the air exchange rates necessary for adequate ventilation for occupants in winter are relatively low and are usually met by the driving produced by the buoyancy force. Mixing ventilation, in which the cold incoming air is tempered by mixing with the internal air, is favoured. In summer, displacement ventilation is preferred as it provides a more efficient way of removing the internal heat gains. Nevertheless, in summer there is often a need for increased ventilation to maintain comfortable internal conditions. These increased rates may then exceed those attainable by buoyancy forces alone and the wind must be harnessed to boost the ventilation. This may be achieved in practice by positioning the low- and high-level openings in regions of positive and negative wind pressure, respectively. For example, positioning a low-level opening on the windward façade and a high-level opening on the roof, or in the lee of the wind, results in a difference in wind pressure between the intake and outlet openings that assists the thermally driven flow. If, however, there is a change in wind direction or if the openings are not suitably located, a situation may arise in which the wind-driven flow opposes the buoyancy-driven flow. It is this situation, and its effect on the thermal stratification produced by a localized source of heat, that we consider in this paper.

In the absence of wind, the steady pattern of ventilation, i.e. the thermal stratification and exchange rates, produced by a localized buoyant source on the floor of an enclosure of height H, with high- and low-level openings has been examined by Linden, Lane-Serff & Smeed (1990). They showed that a turbulent plume sets up a steady two-layer stratification and displacement flow, with a lower layer of depth h at ambient density ρ, and an upper buoyant layer of depth $(H-h)$ with a density equal to the density in the plume at the height of the horizontal interface that separates the layers. The depths of the layers are independent of the buoyancy flux B of the

plume and the direction of the flow through the space is from the lower openings to the upper openings.

Hunt & Linden (2001, referred to hereafter as HL), examine how the ventilation produced by a buoyant plume is modified by an *assisting wind*. By considering an enclosure with upper and lower openings in regions of negative and positive wind pressure, respectively, and separated by a vertical height H, we showed that a steady two-layer stratification is maintained for a range of wind speeds U_{wind} and that the rate of exchange is enhanced with increasing U_{wind}. The depth of the layer at ambient density is set by the relative strengths of the wind- and buoyancy-produced velocities. For a heat source with buoyancy flux B and a building with a pressure drop Δ, this ratio is characterized by the parameter

$$Fr = \sqrt{\frac{\Delta/\rho}{(B/H)^{2/3}}}, \tag{1.1}$$

and the dimensionless 'effective' area of the openings

$$\frac{1}{A^{*2}} = \frac{1}{A_W^{*2}} + \frac{1}{A_L^{*2}}. \tag{1.2}$$

Here the 'effective' area of the openings is defined by

$$A_i^* = \sqrt{2} c_i A_i, \tag{1.3}$$

($i = W, L$) where c is the discharge coefficient that accounts for dissipative losses of the flow through the openings, and A_W and A_L denote the areas of the 'windward' (lower) and 'leeward' (upper) openings, respectively. In general, the value of c depends on the geometry of the opening and the nature of the flow (see Hunt & Holford 2000).

HL express the dimensionless interface height $\xi = h/H$ in terms of Fr and A^*/H^2 as

$$\frac{A^*}{H^2} = \frac{C^{3/2}\xi^{5/3}}{\left((1-\xi)/\xi^{5/3} + CFr^2\right)^{1/2}}, \tag{1.4}$$

where $C = \frac{6}{5}\alpha(9\alpha/10)^{1/3}\pi^{2/3}$ is a constant related to the 'top-hat' entrainment constant α for the plume. An increase in Fr, resulting, for example, from an increase in U_{wind} (and, hence, Δ) or a decrease in B, raises the interface height and decreases the temperature of the buoyant upper layer. Similar effects may also be achieved by increasing A^*/H^2. In contrast to pure buoyancy-driven ventilation, the layer depths are now predicted, and observed, to have a dependence on the buoyancy flux B. The ventilation rate Q is not dependent solely on the magnitude of Fr but depends on the individual values of B and Δ that compose Fr, such that Q increases as Δ and/or B increase, i.e. Q may increase even if Fr decreases.

In this paper we extend the work of Linden *et al.* (1990) and HL by considering steady natural ventilation driven by the *opposing* forces of wind and buoyancy. In § 2 we develop theoretical models of the temperature profiles and ventilation flow rates. We show that an opposing wind allows the possibility of *multiple* steady flow solutions, and the observed flow pattern depends on the time history of the wind and buoyancy changes. For a range of forcing by wind and buoyancy, two stable steady solutions are possible with flow in opposite directions through the space and qualitatively different temperature profiles. Small-scale laboratory experiments designed to reproduce these flows are described in § 3, and the results are compared with the theoretical predictions in § 4. The conclusions are given in § 5.

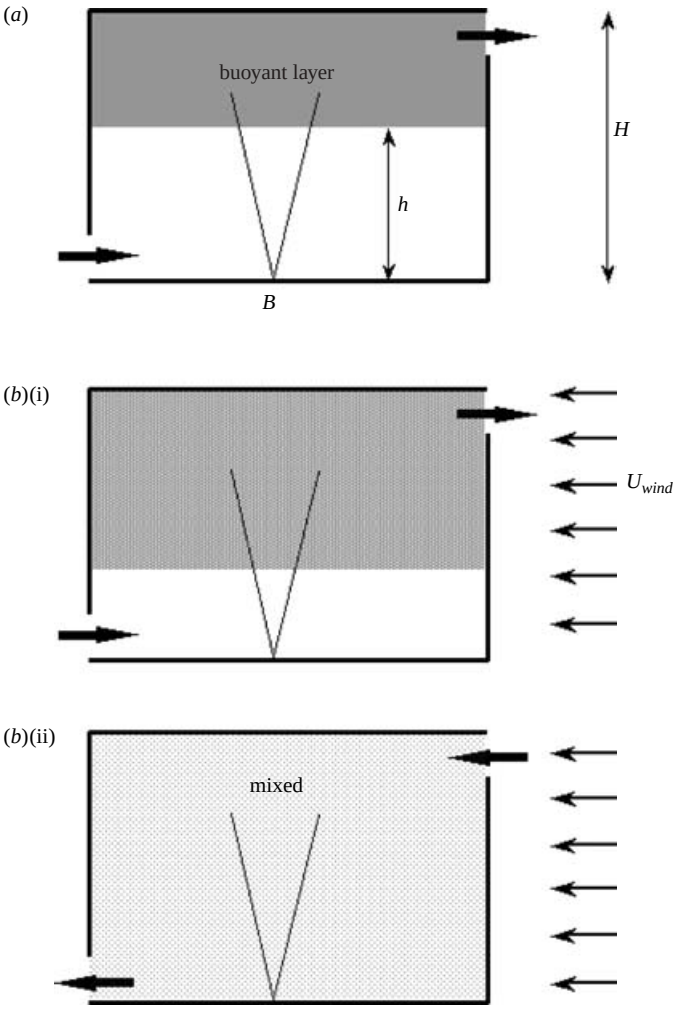

FIGURE 1. (*a*) Displacement flow driven by a localized source of buoyancy at floor level. (*b*) Buoyancy-driven flow opposed by wind, (i) displacement ventilation (weak opposing wind) and (ii) mixing ventilation (strong opposing wind). Note the reversal in the direction of the flow between (i) and (ii).

2. A mathematical model

Consider a single-spaced enclosure (figure 1) of height H with ventilation openings of area A_W located at high level in regions of positive wind pressure, e.g. in the windward façade, and openings of area A_L located at low level in regions of negative wind pressure, e.g. in the leeward façade. Assume that the wind speed U_{wind} is steady and that a high Reynolds number flow around the enclosure creates a drop Δ in wind pressure between the windward and leeward openings. Heat gains within the space are represented as a single steady point source with buoyancy flux B on the floor. The resulting turbulent plume is assumed to be able to rise freely and have a cross-sectional area small compared with that of the enclosure. This point buoyancy source represents an idealized model of a localized heat source found in practice. However, the effect of a finite-area heat source with a non-zero input of momentum flux may be modelled by making a correction for the plume virtual origin (see § 3).

The flow above the source rises as a turbulent plume with reduced gravity G'_p and volume flow rate Q_p given by Morton, Taylor & Turner (1956) as

$$G'_p(z, B) = \frac{B^{2/3}}{Cz^{5/3}} \tag{2.1}$$

and

$$Q_p(z, B) = CB^{1/3}z^{5/3}, \tag{2.2}$$

respectively, where z denotes the vertical distance above the source. There is considerable spread in the empirically determined entrainment coefficient α reported in the literature, and interface heights and ventilation flow rates are sensitive to the value chosen (see HL). In this model we take a value appropriate for a top-hat plume $\alpha = \sqrt{2} \times 0.083 = 0.117$ (Turner 1986; Linden 2000).

In the absence of wind, the buoyant plume creates a warm layer of fluid near the ceiling and the resulting hydrostatic pressure difference between the inside and outside of the enclosure drives buoyant fluid out through upper openings and draws denser ambient fluid in through lower openings (Linden *et al.* 1990). There is an initial transient period (Hunt & Linden 1998; Kaye & Hunt 2004) during which the depth and temperature of the upper layer increase and after some time a steady flow with a two-layer stratification is established.

If the driving forces of wind and buoyancy are considered in isolation, the wind will drive a flow through the space from the high-level to the low-level openings, in the direction shown in figure 1(*b*)(ii). On the other hand, the buoyancy forces will drive a flow in the opposite direction, from the low-level to the high-level openings, as shown in figure 1(*a*). The situation considered is, therefore, one in which the wind opposes the buoyancy-driven flow. In this case, with a change in either wind speed or the heat source, the ventilation will undergo a transient adjustment before a steady flow is established. The resulting steady ventilation flow will depend on the change in wind speed, the timescale over which the wind is increased, the strength of the buoyant source and the geometry of the enclosure. For weak opposing winds, we expect that the basic steady two-layer stratification established in the absence of wind will be maintained (figure 1*b*(i)), with leeward openings acting as inlets and windward openings as outlets. In this case and for small increases in wind speed we assume that the two-layer stratification is maintained provided the interface lies above the lower opening.

At larger wind speeds, or for sufficiently large changes in wind speed, wind-driven air enters the enclosure through windward openings and drives fluid out through openings in the lee. In this case there are two possibilities. For 'intermediate' wind speeds there is only a small loss of buoyancy from the enclosure, and the rate at which buoyancy accumulates in the space exceeds the rate at which buoyancy is lost through leeward openings. There is a net increase in buoyancy, which reduces and finally stops the wind-driven inflow and the flow reverts to a steady displacement flow. For 'strong' wind speeds the rate at which buoyancy is lost from the enclosure exceeds the rate at which buoyancy is supplied, there is a net decrease in buoyancy, and the stratification is broken down. A steady mixing flow (figure 1*b*(ii)), with an interior at approximately uniform temperature, is established, in which the flow direction remains in the opposite sense to the wind-opposed displacement flow.

2.1. *Small opposing wind*

When a two-layer stratification is maintained, the steady volume flow rate Q that results from a wind pressure drop Δ opposing the flow induced by a buoyant upper

layer of depth $(H-h)$ and density difference $\Delta\rho$ is given by

$$Q = \left(Q_B^2 - Q_W^2\right)^{1/2}, \tag{2.3}$$

where

$$Q_W = A^* \left(\frac{\Delta}{\rho}\right)^{1/2} = A^* Fr \left(\frac{B}{H}\right)^{1/3} \tag{2.4}$$

and

$$Q_B = A^*(g'(H-h))^{1/2} \tag{2.5}$$

denote the wind-driven and buoyancy-driven volume fluxes, respectively. In (2.5) $g' = g\Delta\rho/\rho$ is the reduced gravity of the buoyant layer. Equations (2.3)–(2.5) are obtained from the analysis presented by HL for wind-assisted flows, taking into account the reversal in wind direction. It is assumed that the density difference $\Delta\rho$ between the fluid in the homogeneous buoyant upper layer and the ambient fluid is small compared with the ambient density ρ (as is the case for typical ventilation flows) so that the Boussinesq approximation is valid. From (2.3)–(2.5), we note that Q may be expressed as

$$Q = A^* g'^{1/2} \left(H - h - \frac{\Delta}{\rho g'}\right)^{1/2}, \tag{2.6}$$

and thus an opposing wind effectively reduces the driving head of buoyant fluid by a height $\Delta/\rho g'$. The dependence of Q on B, Δ, h, H and A^* may be obtained directly from (2.3)–(2.5), where on substituting $g' = B/Q$, we obtain the cubic

$$\left(\frac{Q}{Q_W}\right)^3 + \frac{Q}{Q_W} - \frac{1}{F^3}\left(1 - \frac{h}{H}\right)^2 = 0, \tag{2.7}$$

where

$$F = \left(\frac{\Delta}{\rho}\right)^{1/2} \left(\frac{A^*}{BH}\right)^{1/3} = Fr \left(\frac{A^*}{H^2}\right)^{1/3}. \tag{2.8}$$

This last equation shows that F is the essential parameter describing the flow. Since it includes the effective opening area A^*, F is the ratio of the wind-induced and buoyancy-induced velocities *within the enclosure*.

When the enclosure is completely filled with buoyant fluid the buoyancy-driven ventilation flow rate $Q_B = A^*(g'H)^{1/2}$. Since the buoyancy flux B supplied equals the buoyancy flux through the openings then we can write $Q_B = A^*(BH/A^*)^{1/3}$. Consequently, the buoyancy-driven velocity in (2.8) is the maximum velocity that can be driven by buoyancy if the enclosure was completely filled with buoyant fluid.

2.2. *Large opposing wind*

For a sufficiently large opposing wind, the stratification is broken down and the interior is assumed well mixed, so that

$$Q_B = A^*(g'H)^{1/2}. \tag{2.9}$$

The wind-driven component Q_W is given by (2.4). For large opposing winds $Q_W > Q_B$, $Q < 0$ and satisfies

$$Q = -\left(Q_W^2 - Q_B^2\right)^{1/2}. \tag{2.10}$$

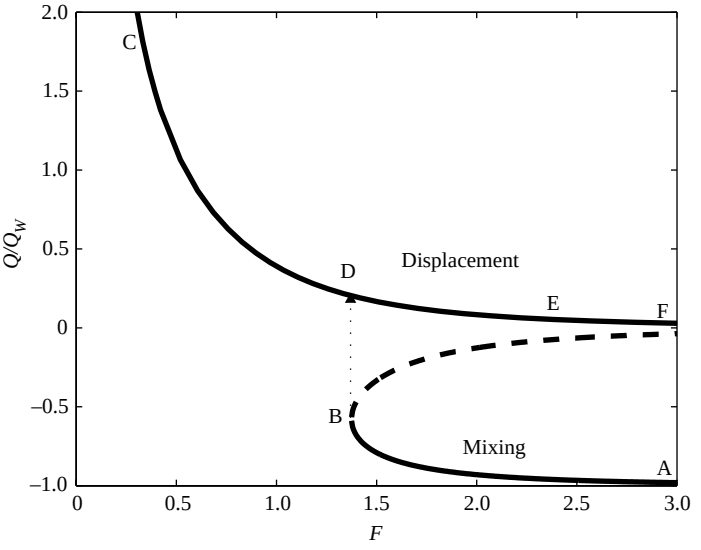

FIGURE 2. Q/Q_W plotted against F for $A^*/H^2 = 0.05$. The solution for $Q/Q_W > 0$ represents displacement flow. The solution for $Q/Q_W < 0$ represents mixing flow – the solid curve indicates the stable branch and the dashed curve shows the unstable branch.

Substituting $g' = B/|Q|$ into (2.10) we obtain

$$\left(\frac{Q}{Q_W}\right)^3 - \frac{Q}{Q_W} - \frac{1}{F^3} = 0. \tag{2.11}$$

Dimensionless volume flow rates for both steady mixing flows (2.11), and steady displacement flows (2.7), are shown in figure 2 (see § 2.3 for the dependence of h on F). Displacement ventilation occurs when $Q/Q_W > 0$ and mixing ventilation when $Q/Q_W < 0$. For the displacement flow, (2.7) has three real solutions, two negative (hence unphysical) for all values of F. For the mixing flows, (2.11) has one positive real root (hence unphysical) or two negative real or two complex roots depending on the value of F; this is examined in § 2.4.

Figure 2 shows that there are three solutions, two corresponding to mixing ventilation and one corresponding to displacement ventilation. The solution branches plotted as solid lines are stable, while the dashed curve represents an unstable mixing branch. This unstable branch is characterized by a small flow rate Q and a large interior buoyancy g'. On this unstable branch, an increase in the magnitude of Q leads to a heat loss, and as a result g' decreases and, consequently, Q increases further, and the system moves to the stable mixing branch. A decrease in g' reduces the buoyancy driving, increases Q, which, in turn, decreases g' further. Similarly, a decrease in Q is amplified, and the system switches back to the displacement branch. Similar arguments show that the branch AB on figure 2 is stable to small perturbations, and so we expect the system to exhibit solutions only on the stable mixing branch AB or the displacement branch CF.

The transition from mixing to displacement flow occurs as follows. Consider constant wind and no heat source ($B = 0$); this case corresponds to a stable mixing flow with an infinite F (point A on figure 2). In this purely wind-driven limit the flow rate $Q/Q_W = -1$. When B is increased from zero, F decreases, and the steady solution

falls on the curve between points A and B. The buoyancy-driven volume flux opposing the wind increases in magnitude as B increases and, hence, $|Q/Q_W|$ decreases. At a critical value of B, corresponding to $F = F_c$ (point B), the wind is unable to maintain mixing flow for any further increase in B, which then results in a transition from mixing to displacement flow (from point B to D on figure 2). This results in a reversal in the direction of flow through the space and a significant reduction in $|Q/Q_W|$. If the buoyancy flux B is increased still further, the steady solution moves along the displacement flow branch from point D to C (C represents the case $F = 0$).

If, on the other hand, the enclosure contains a source with finite $B > 0$ and the wind speed is initially zero, so that $F = 0$ and $Q_W = 0$, there is a displacement flow – point C on figure 2. Suppose the wind speed is now increased; F increases and the wind-driven component of the volume flow rate increases so that Q/Q_W decreases and buoyancy accumulates in the space. This behaviour continues until $F > F_c$. At some value of $F > F_c$ (point E), which depends on the specific geometry of the space and the openings, net buoyancy is lost from the space (by flow out of the lower openings), and the system makes a transition to an unstable mixing flow in which flow rates are weak and the reduced gravity of the interior is large. As explained above, this state is unstable and the solution moves to the stable mixing branch AB, with high flow rate and small buoyancy. The corresponding solution for the reduced gravity as a function of F is considered in § 2.4.

2.3. *Steady-state displacement flow*

Consider a gradual increase in wind speed, from zero to a fixed value U_{wind}. As the wind speed increases the external pressure on the windward façade increases and exceeds the hydrostatic (stack) pressure difference induced by the buoyant layer. This excess pressure drives dense fluid in through windward openings and expels ambient fluid from the lower layer through leeward openings. The dense inflow that enters at high level mixes with and increases the depth of the buoyant layer. As this layer increases in depth it is supplied with increasingly buoyant fluid from the plume. This increases the stack pressure until, after some time, it is again sufficient to drive a flow out through the windward openings and into the oncoming wind. A steady flow is re-established when the volume and buoyancy fluxes in the plume at the new level $z = h$ of the interface are balanced by the volume and buoyancy fluxes driven through the upper openings. The depth and reduced gravity of the upper layer are then both greater than the no-wind case, but the ventilation flow rate is reduced.

In order to determine the steady stratification and flow rate we follow the approach presented by HL. We match the volume and buoyancy fluxes in the plume at the position of the interface with the volume and buoyancy fluxes driven through the space by the buoyant upper layer and the wind. Substituting (2.1) and (2.2), evaluated at $z = h$, into (2.6), the depth of the ambient layer as a fraction of the total height of the space $\xi = h/H$ may be expressed as

$$\frac{A^*}{H^2} = \frac{C^{3/2}\xi^{5/3}}{\left((1-\xi)/\xi^{5/3} - CF^2(H^2/A^*)^{2/3}\right)^{1/2}} = \frac{C^{3/2}\xi^{5/3}}{\left((1-\xi)/\xi^{5/3} - CFr^2\right)^{1/2}}, \tag{2.12}$$

where F is defined in (2.8). From (2.1) and (2.2) the reduced gravity of the upper layer and the ventilation flow rate are

$$\frac{g'}{G'_H} = \xi^{-5/3} \tag{2.13}$$

and

$$\frac{Q}{B^{1/3}H^{5/3}} = C\xi^{5/3}, \tag{2.14}$$

respectively, where $G'_H \equiv G'_p(z = H, B)$ is the reduced gravity of the plume at the ceiling.

Figures 3 and 4 show the effect of F and A^*/H^2, respectively, on the stratification and exchange rates. For a fixed value of A^*/H^2, $\xi = h/H$ decreases as F is increased (figure 3*a*), g'/G'_H increases (figure 3*b*) and $Q/(B^{1/3}H^{5/3})$ decreases (figure 3*c*). The increase in g'/G'_H and upper-layer depth with increasing F implies an increase in the buoyancy-driven flow Q_B (see (2.5)). To emphasize the effect of F on the ventilation these results are re-plotted in figure 4 with A^*/H^2 as the parameter. Note that the effect of an increase in F on h/H, g'/G'_H and $Q/(B^{1/3}H^{5/3})$ is more dramatic as A^*/H^2 is increased, i.e. enclosures with large openings are more influenced by wind than those with smaller openings – see figure 4(*c*). The values of F span the critical value $F_c = 1.37$ (see § 2.4), and plots show that for $F = 2$ displacement ventilation is maintained but for the smaller values of F the interface reaches the ceiling and mixing ventilation occurs.

2.4. *Steady-state mixing flow*

A change in wind speed or direction, rate of buoyancy input or opening area that results in a loss of buoyancy through low-level openings exceeding the buoyancy supply, cools the space. Wind effects become more significant with time, a displacement flow cannot be maintained, and mixing ventilation occurs. In mixing flow the interior fluid outside the plume is well mixed. In this case conservation of volume and buoyancy require

$$Q^L = Q^W = |Q| \tag{2.15}$$

and

$$B = |Q|g', \tag{2.16}$$

where Q^L and Q^W denote the steady volume fluxes through leeward and windward openings, respectively. The steady reduced gravity is defined as

$$g' = g\frac{(\rho - \rho_b)}{\rho}, \tag{2.17}$$

where ρ denotes the density of the exterior fluid and ρ_b denotes the (uniform) density of the interior fluid. Applying conservation of momentum over a control volume containing the windward and leeward openings and using the neutral pressure level, we obtain

$$Q = -A^*\sqrt{\frac{\Delta}{\rho} - g'H}. \tag{2.18}$$

(The analysis for a buoyancy source with non-zero source mass flux is outlined in Appendix A.)

In non-dimensional terms

$$\frac{Q}{Q_W} = -\frac{1}{F}(F^2 - G')^{1/2} = -\left(1 - \frac{G'}{F^2}\right)^{1/2}, \tag{2.19}$$

where

$$G' = \frac{g'A^{*2/3}H^{1/3}}{B^{2/3}}. \tag{2.20}$$

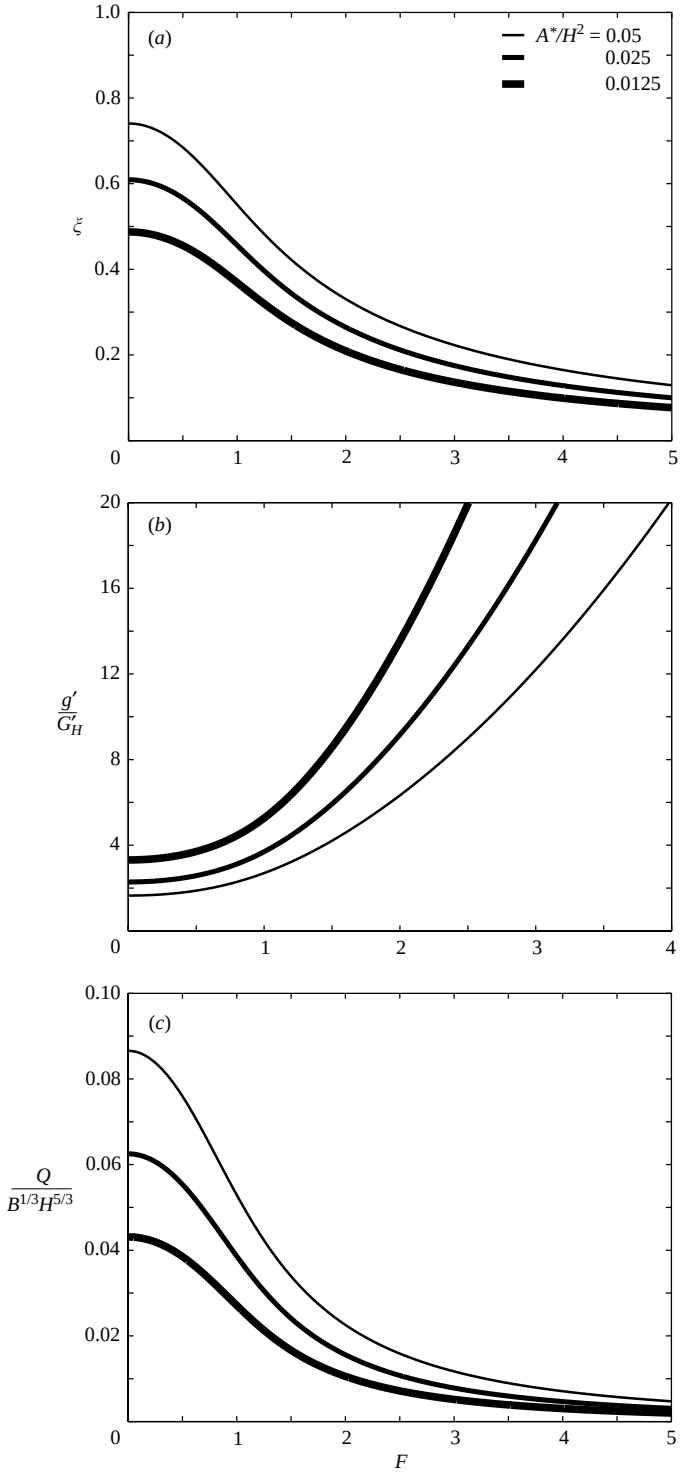

FIGURE 3. Displacement flow: dimensionless values of (*a*) the interface height $\xi = h/H$, (*b*) the upper-layer buoyancy g'/G'_H and (*c*) the flow rate $Q/(B^{1/3}H^{5/3})$ plotted against F, for different values of the dimensionless area A^*/H^2. (G'_H is the reduced gravity in the plume at the ceiling a distance H from its source.)

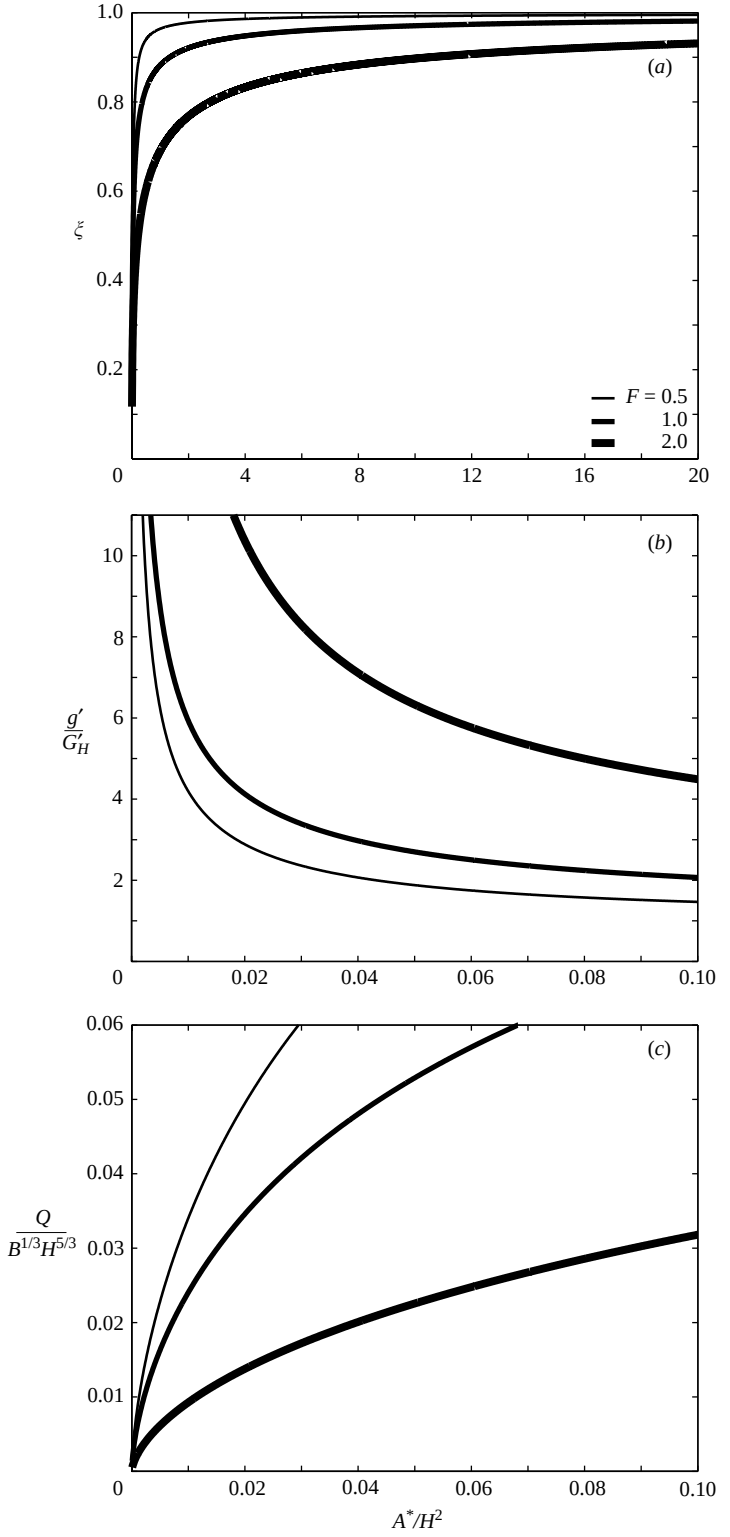

FIGURE 4. Displacement flow: dimensionless values of (*a*) $\xi = h/H$, (*b*) g'/G'_H and (*c*) $Q/(B^{1/3}H^{5/3})$ plotted against A^*/H^2, for different values of F.

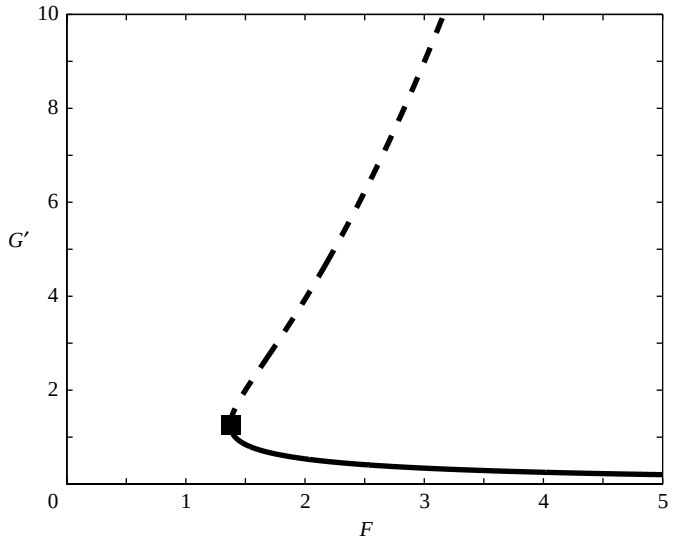

FIGURE 5. Mixing flow: dimensionless buoyancy G', defined by (2.20), plotted against F. The dashed line shows the unstable solution. The square indicates the minimum value of F, namely $F = F_c$, for which a stable mixing flow is maintained.

Substituting $|Q| = B/g'$ into (2.19) and using $Q_W = A^{*2/3}(BH)^{1/3}F$, from (2.4) and (2.8), shows that the reduced gravity is given by the solution of

$$G'^3 - G'^2F^2 + 1 = 0. \tag{2.21}$$

The variation of G' with F (figure 5) shows that for $F = F_c$ there is a unique solution (marked by a square) and, for $F > F_c$, there are two possible steady values of G' for a given F; the lower of the two values corresponds to the stable mixing flow and the upper to the unstable mixing flow. On the stable branch, for $F \gg 1$ we have $G' < 1$ and we obtain from (2.21)

$$G' \approx \frac{1}{F}. \tag{2.22}$$

From (2.21), F may be expressed in terms of G' as

$$F = \left(\frac{1}{G'^2} + G'\right)^{1/2}, \tag{2.23}$$

and, hence, from $\mathrm{d}F/\mathrm{d}G' = 0$, the reduced gravity at F_c is given by

$$G'(F = F_c) = 2^{1/3} = 1.2599, \tag{2.24}$$

which is the maximum value the reduced gravity can take while maintaining a mixing flow. Substituting (2.24) into (2.21) we find that

$$F_c = \frac{\sqrt{3}}{2^{1/3}} = 1.3747. \tag{2.25}$$

Thus at this critical condition the wind-induced flow in the space is about 40% larger than the buoyancy-driven flow.

The variation of Q/Q_W with F as shown in figure 6 illustrates the two possible flow rates for $F > F_c$. The larger value of $|Q/Q_W|$ corresponds to the stable mixing flow.

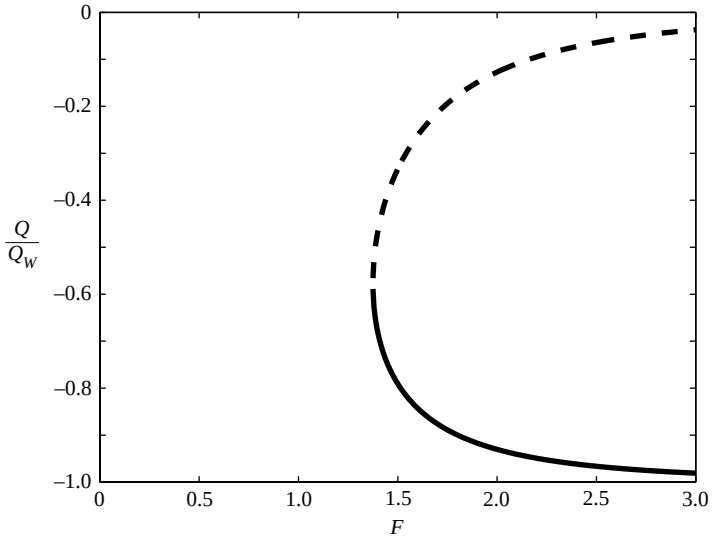

FIGURE 6. Mixing flow: the dependence of Q/Q_W on F. The dashed line shows the unstable solution. The minimum flow rate for which a mixing flow can be maintained occurs at $F = F_c = 1.3747$ and is $|Q/Q_W| = 0.5773$.

When $F = F_c (= 3^{1/2}/2^{1/3})$, $G' = 2^{1/3}$, hence from (2.19)

$$\frac{Q}{Q_W} = -3^{-1/2} = -0.5773. \tag{2.26}$$

This value represents the minimum possible volume flow rate at which a stable mixing flow can be maintained.

Note that for $F \gg F_c$, (2.19) yields

$$\frac{Q}{Q_W} = -1 + \frac{G'}{2F^2}, \tag{2.27}$$

for $|G'/F^2| < 1$. Substituting G' from (2.22) into (2.27) shows that the volume flow rate, in terms of F, is given by

$$\frac{Q}{Q_W} = -1 + \frac{1}{2F^3}, \tag{2.28}$$

for $F \gg 1$.

In summary, in a stable mixing mode the effect of an increase in the buoyancy flux is to decrease the flow rate and increase the reduced gravity. The lower value of Q/Q_W corresponds to the unstable mixing regime.

The full solution for the reduced gravity as a function of F is depicted in figure 7. Note that, for a given room and opening geometry, the layer produced by displacement flow is always warmer (higher G') than the mean temperature produced by mixing ventilation irrespective of F. The figure re-iterates that a single steady temperature is possible for $F < F_c$ while for $F \geqslant F_c$ two (stable) temperatures are possible. Thus a range of temperatures are unobtainable within the space for a given Fr, and varying A^*/H^2 provides the only means of temperature regulation. Cooling is achieved as the vent area is increased.

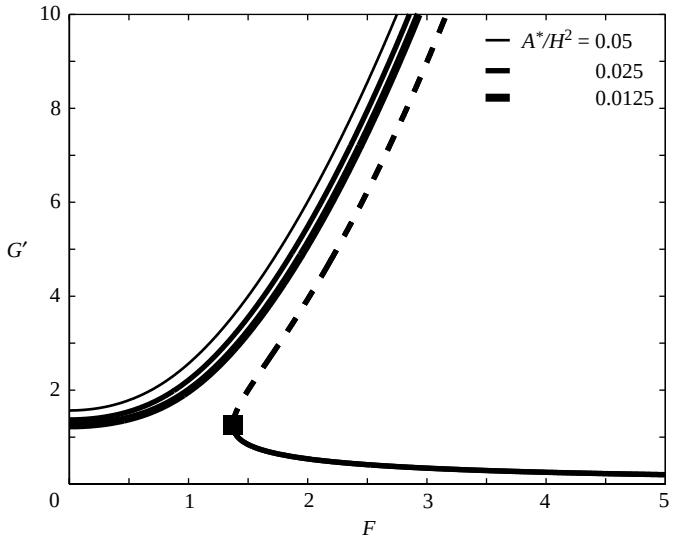

FIGURE 7. G' plotted against F. The square located on the mixing flow branch marks the critical value F_c and the dashed line the unstable mixing branch. The remaining branches are the corresponding displacement flow solutions for $A^*/H^2 = 0.0125, 0.025$ and 0.05.

The theory developed in this section is applied to a typical building geometry in Appendix B; the example given compares wind-opposed and pure-buoyancy-driven ventilation, as well as the wind-assisted case (cf. the example given in HL).

3. Experiments

A transparent Perspex box of uniform internal cross-section 0.295 m × 0.15 m and height 0.25 m was used to represent a generic single-spaced enclosure. Five circular holes (diameter 20 mm) in the windward and leeward sides of the box at low/high levels, respectively, provided connections between the interior and the surroundings. Windward and leeward openings were separated by a vertical distance of 0.21 m. The total opening area was varied by blocking the holes with plastic bungs.

The box was positioned in the test section of a flume tank (cross section 2.65 m × 0.30 m and height 0.57 m) containing fresh water. Wind flow past the enclosure was represented by a mean flow in the flume. The mean speed of the flow could be varied, and this allowed a range of different wind speeds to be considered. For each 'wind' speed the dynamic pressure drop Δ between the windward and leeward openings was measured using a simple oil–water manometer (Hunt & Linden 1997). Pressure fluctuations of between 5% and 10% of the mean pressure drop were recorded and, as expected, the pressure drop varied with the square of the 'wind' speed. Our primary measurement was the wind pressure drop and we only measured the speed to confirm the speed/pressure relationship. Writing P_i and P_o for the pressures on the inlet and outlet openings, respectively, we have

$$P_i = C_{pi}\tfrac{1}{2}\rho U_{wind}^2, \tag{3.1}$$

$$P_o = C_{po}\tfrac{1}{2}\rho U_{wind}^2, \tag{3.2}$$

where C_{pi} and C_{po} denote pressure coefficients and

$$\Delta = P_i - P_o = \tfrac{1}{2}\rho U_{wind}^2(C_{pi} - C_{po}). \tag{3.3}$$

Heat gains were represented by supplying salt solution, via a constant-head tank, through a circular nozzle (diameter $D = 5\,\text{mm}$) mounted on the upper face of the box. The nozzle (described in detail in HL) was designed to produce a turbulent plume close to the point of release. The supply flow rate was measured with an in-line flow meter and finely adjusted by means of a needle valve. The strength of the buoyancy source was increased by increasing either the density or the flow rate of the supply. Supply flow rates were typically 1–$3\,\text{cm}^3\,\text{s}^{-1}$ and reduced gravities were typically 500–$2000\,\text{mm}\,\text{s}^{-2}$. The distance between the exit point of the nozzle and the bottom of the box was $H_m = 0.232\,\text{m}$.

Flows were either back-lit or visualized with a shadowgraph. Dye (food colouring) was added to the salt solution and acted as a surrogate for the salt concentration. The light source and the camera (a COHU CCD camera) were positioned approximately 8.5 m behind and 2.5 m in front of the tank, respectively. Parallax errors were estimated to be less than 1 mm with the shadowgraph and less than 4 mm when the flow was back-lit.

For displacement flows, measurements of the depth of the interface and the density contrast across it were taken once a steady flow was established. Samples of fluid were extracted from the upper and lower layers using a needle syringe and their densities measured using a densitometer. For mixing flows, three samples were extracted from different regions of the box (in each case outside the plume region). The samples were used to determine the uniformity of the interior and to provide an average value for the reduced gravity. The differences in density between the samples was typically 5% of the predicted density in the plume at the bottom of the box (from (2.1)). The assumption that the interior fluid (outside the plume region) is uniformly well mixed is, therefore, a reasonable one. The results plotted in § 4 are based on the average of the three density measurements. A sample of fluid was also taken from the flume to account for the (small) variation in the background density that occurs as the saline solution released from the box mixes with the fresh water in the flume.

Before comparing the observations with the theoretical predictions of § 2, a correction was made to the measured interface height h_m and to the parameter F to account for the non-ideal source conditions of the saline plume. In contrast to the idealized plume assumed in § 2, the saline plume issues from a source of finite area with non-zero initial fluxes of volume $Q_{p0} \equiv Q_p(z=0)$ and momentum M_0. The correction, in the form of a virtual origin located a distance z_v behind the actual plume origin (at $z=0$), effectively increases the height of the box such that the corrected non-dimensional interface height $\widehat{h}/\widehat{H}$ is given by

$$\frac{\widehat{h}}{\widehat{H}} = \frac{h_m + z_v}{H_m + z_v}. \tag{3.4}$$

As F depends on the height of the enclosure we define the corrected parameter $\widehat{F}$ as

$$\widehat{F} = \left(\frac{\Delta}{\rho}\right)^{1/2} \left(\frac{A^*}{B\widehat{H}}\right)^{1/3}. \tag{3.5}$$

Symbols marked with a 'hat' signify that the quantity has been determined based on the 'effective' height $H_m + z_v$, rather than the actual height H_m, of the enclosure, and are referred to as 'corrected' in the figures. Following Hunt & Kaye (2001), a plume with source conditions (Q_{p0}, M_0, B_0) may be replaced with an equivalent point-source pure plume with source conditions $(0, 0, B_0)$ at a virtual origin $z = -z_v$; see their equation (34). In Hunt & Kaye (2001), the parameter Γ (their equation (25))

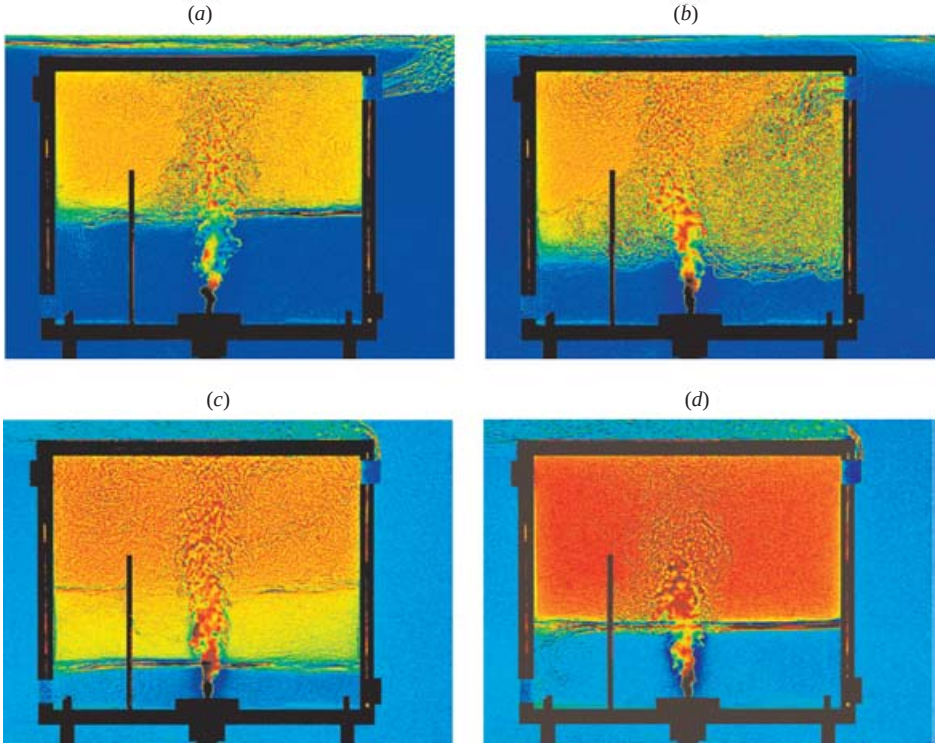

FIGURE 8. For caption see facing page.

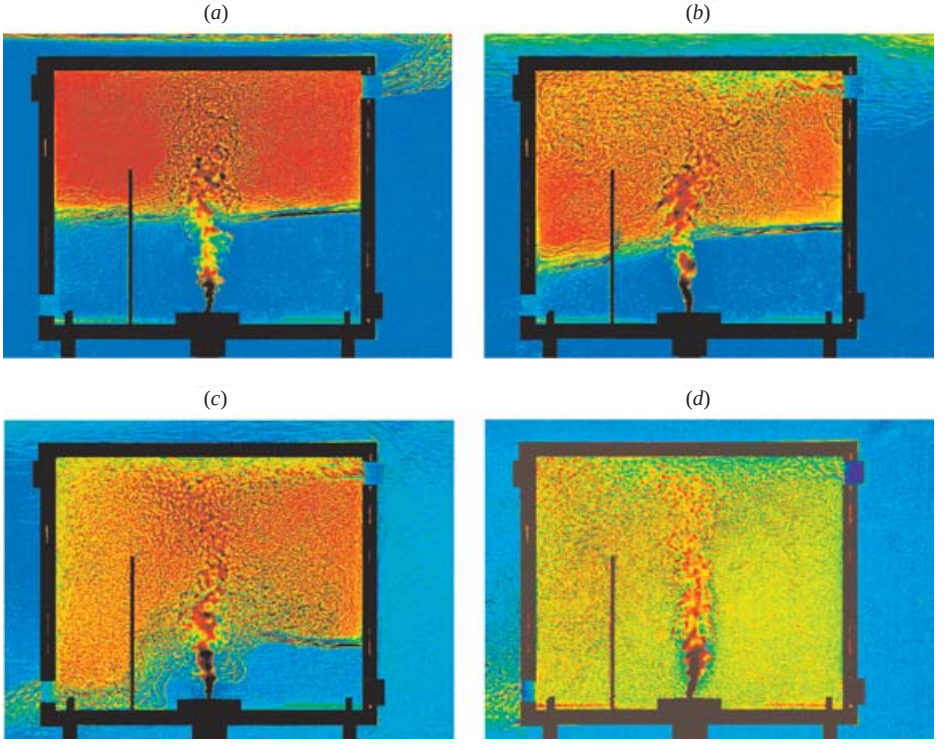

FIGURE 12. For caption see facing page.

which characterizes the source conditions is appropriate for Gaussian profiles. For the top-hat profiles assumed here $\Gamma = 5Q_{p0}^2 B_0/8\alpha\pi^{1/2}M_0^{5/2}$. The source conditions used gave z_v of about $1D$ to $3D$.

4. Results

In the absence of wind, the saline plume descended and spread out on reaching the base of the box to form a dense layer. Fluid from this layer flowed out through the lower openings and was replaced by an inflow of fresh ambient fluid which entered through upper openings. Little mixing was observed and a displacement flow and two-layer stratification was established. Figure 8(*a*) depicts a typical steady displacement flow.

With a wind opposing the buoyancy-driven flow, one of two distinct steady flow regimes was established depending on F and A^*/H^2. For a fixed A^*/H^2, a two-layer stratification and displacement flow was maintained as the wind speed was increased (from zero) in steps for a range of F. For $F > F_c$ a reversal in the flow direction was observed, the stratification was broken down, and the interior became well mixed. For both displacement and mixing flows the effects of Δ (or, equivalently, U_{wind}), B and A^*/H^2 on the behaviour of the flow were investigated. Results of these experiments are now described.

4.1. *Displacement flow*

4.1.1. *Effect of wind speed*

A steady two-layer stratification was set up by the plume and the 'wind' speed then increased in discrete steps. The typical transient stages of the flow, from the steady two-layer displacement flow established by the plume (figure 8*a*) to the steady flow established in the presence of an opposing wind (figure 8*d*), are depicted in figures 8(*b*) and 8(*c*). Qualitative differences were observed in the transient behaviour depending on the magnitude of the change in wind speed as discussed later.

For relatively large changes in U_{wind}, an inflow of ambient fluid was observed through the windward openings, stopping the outflow and producing a plume that broke through the interface and deposited a layer of intermediate-density fluid above it (figure 8*c* – note the figure depicts the inverted flow). The intermediate layer continued

FIGURE 8. Enhanced and inverted false-colour shadowgraph images showing the transition from a steady buoyancy-driven displacement flow to a steady buoyancy-driven displacement flow opposed by wind, at times (*a*) $t = 0$ s, (*b*) $t = 25$ s, (*c*) $t = 90$ s and (*d*) $t = 465$ s after the wind was applied. $B = 147\,\mathrm{cm^4\,s^{-3}}$ and $A^*/H^2 = 1.46 \times 10^{-2}$. In (*a*) there is no wind. In (*b*), (*c*) and (*d*) the wind direction is from right to left, with $Fr \approx 3.15$, i.e. $F \approx 0.77$. In (*a*), (*c*) and (*d*) inflow of ambient fluid is through lower openings (bottom left) and outflow of saline solution is through upper openings (top right). In (*b*) inflow is through upper openings and outflow is through lower openings. (*a*) and (*d*) depict the steady initial and final flows. The vertical line is a perforated barrier used to deflect the inflow away from the path of the plume, to avoid the disruption of the plume.

FIGURE 12. Enhanced and inverted shadowgraph images showing the transition from a steady displacement flow driven solely by buoyancy forces to a steady mixing flow established by an opposing wind. (*a*) $t = 0$ s, (*b*) $t = 5$ s, (*c*) $t = 15$ s and (*d*) $t = 615$ s. $B = 146.5\,\mathrm{cm^4\,s^{-3}}$ and $A^*/H^2 = 1.46 \times 10^{-2}$. In (*a*) there is no wind. In (*b–d*) the wind direction is from right to left, with $Fr \approx 7.40$, i.e. $F \approx 1.81$. In (*a*) inflow of ambient fluid is through lower openings (bottom left) and outflow of saline solution is through upper openings (top right). In (*b–d*) the direction of flow is reversed. (*a*) and (*d*) depict the steady flows.

to increase in depth when there was inflow through the windward openings. Provided the upper interface remained below the level of the leeward openings, buoyant fluid was unable to drain from the enclosure, and the hydrostatic head increased as a result of the continuous supply of buoyant fluid from the plume. In this case, the inflow of ambient fluid decreased and eventually stopped. The intermediate layer was then entrained into the plume and the system reverted to a steady two-layer displacement flow with a deeper and denser saline layer each time the wind speed increased. For relatively small changes in wind speed an exchange flow, of predominantly outflow, occurred at the windward openings. With this weak inflow a clear three-layer stratification was not observed during the transients. For even smaller changes in wind speed, inflow through windward openings was not observed. In both these cases the depth of the buoyant layer was observed to increase as a result of the inhibition of the buoyancy-driven ventilation by the opposing wind.

For larger values of the change in wind speed the interface rose above the level of the leeward openings allowing some buoyant fluid to leave the enclosure. If the buoyancy flux of this outflow was small compared with the buoyancy flux of the plume then the net buoyancy in the enclosure continued to increase and, after some time, the outflow ceased, and the flow reverted to a steady displacement flow. On the other hand, if the buoyancy flux expelled from the enclosure exceeded the source buoyancy flux, the net buoyancy in the enclosure decreased with time, the interface rose to the top of the box, and a mixing flow was established.

The dimensionless steady interface height ξ and lower-layer reduced gravity G' are plotted against F in figure 9. As F, or equivalently U_{wind}, increases, ξ decreases implying a reduction in the ventilation flow rate. An increase in F increases G'. The results show that as F approaches F_c changes in wind speed result in increasingly large changes in ξ. Agreement between the experiment and theoretical predictions of § 2 is good. Comparison of the solid and hollow square symbols in figure 9 shows that the variation of ξ and G' against F exhibit similar trends at a smaller value of $A^*/\widehat{H}^2$.

Qualitative differences were observed in the transient behaviour depending on the magnitude of the change in wind speed. If the wind speed increased gradually, buoyancy accumulated in the space and opposed the strengthening wind. Consequently, a relatively large value of F was required to flush the buoyancy from the space and set up a mixing flow. In contrast, sudden relatively large increases in wind speed rapidly flushed buoyancy from the space and a mixing flow established at a lower wind speed. This is one of the complexities of the displacement–mixing transition, see § 4.3.

Good agreement between experiment and predictions is achieved using $\alpha = 0.117$ (Turner 1986) and constant values for the discharge coefficients c, taken to be 0.6. Measurements (Hunt & Holford 2000) demonstrate that c exhibits some dependence on density contrast, but these effects are likely to be small here and we are unable to detect them in our experimental data.

4.1.2. *Effect of opening area*

In some experiments B and Δ were fixed and the steady position of the interface and the lower-layer reduced gravity measured for a range of opening areas. Results for $Fr = 3.5$, showing, (*a*) $\widehat{h}/\widehat{H}$ vs. $A^*/\widehat{H}^2$ and (*b*) $\widehat{G}'$ vs. $A^*/\widehat{H}^2$ are presented in figure 10. As $A^*/\widehat{H}^2$ increases, $\widehat{h}/\widehat{H}$ increases (figure 10*a*) and $\widehat{G}'$ increases (figure 10*b*). The former result implies an increase in Q – see (2.14). On increasing $A^*/\widehat{H}^2$ still further it was possible to break down the stratification and establish a steady mixing flow.

Increasing the area of the openings assists the buoyancy-driven and the wind-driven components of the ventilation by the same factor. This may explain the gradual

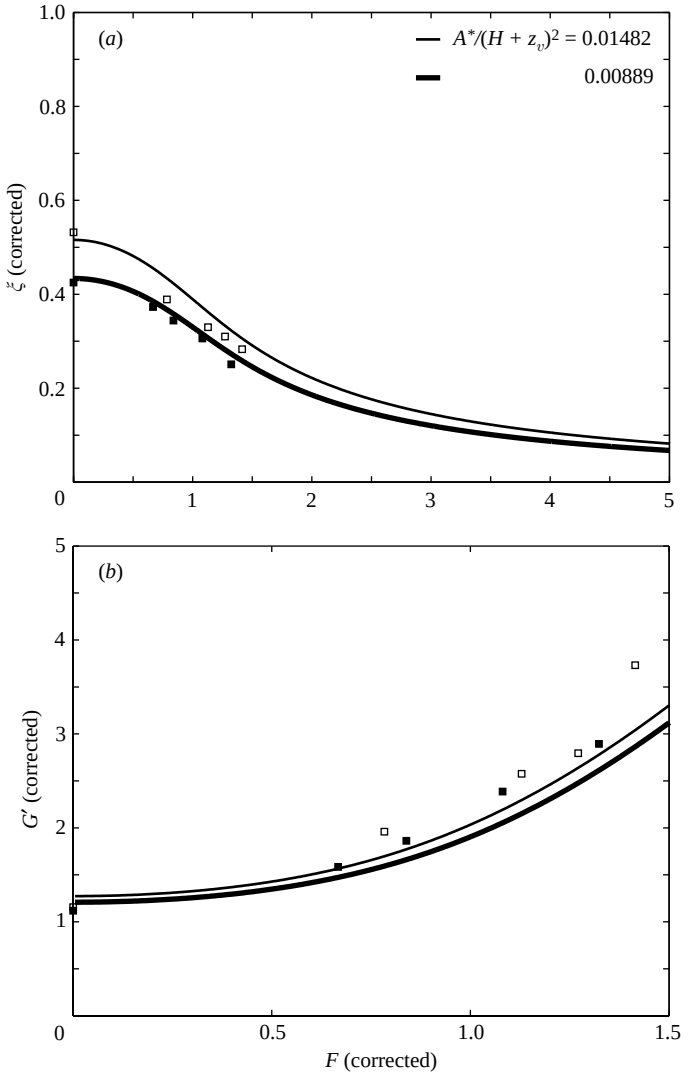

FIGURE 9. Displacement flow – effect of wind speed on (*a*) ξ and (*b*) G'. The heavy and light lines are predictions for different opening areas and correspond to the data points shown as solid and hollow squares, respectively.

transition of the flow from displacement to mixing ventilation. Displacement flows, however, may be maintained at higher winds by reducing the opening area. For example, with $A^*/\widehat{H}^2 \approx 0.021$ a transition from displacement to mixing occurred in the interval $Fr_c = 5.65$–6.22, i.e. $F_c = 1.53$–1.69. When $A^*/\widehat{H}^2$ was reduced, by approximately a factor of two, to $A^*/\widehat{H}^2 = 0.0123$ a transition from displacement to mixing occurred for $Fr_c = 6.27$–6.84, i.e. $F_c = 1.45$–1.58. Note that as expected the value of F at which transition to mixing occurs exceeds the value of $F_c = 1.37$ at which the transition to displacement from mixing is predicted. The intervals in F_c given above were based on incremental increases in the wind pressure drop of less than 30%, i.e. simulating a gradually strengthening wind.

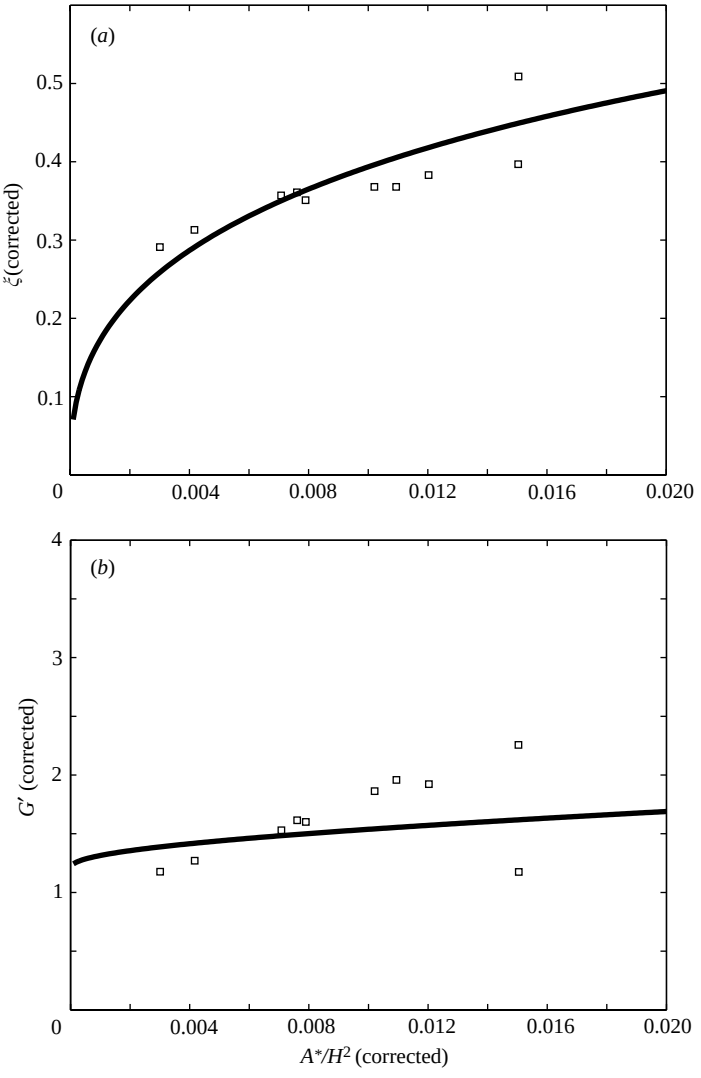

FIGURE 10. Displacement flow – effect of opening area on (*a*) ξ and (*b*) G'. The experiments (squares) and theoretical curves are for $Fr = 3.5$.

4.1.3. *Effect of buoyancy flux*

The effect of the buoyancy flux on the stratification is shown in figure 11 where the dimensionless height $\widehat{h}/\widehat{H}$ in (*a*) and buoyancy $g'/(\Delta/\rho\widehat{H})$ in (*b*) are plotted against the dimensionless buoyancy flux $B/\widehat{H}(\Delta/\rho)^{3/2}$ for $A^*/\widehat{H}^2 = 1.23 \times 10^{-2}$. As $B/\widehat{H}(\Delta/\rho)^{3/2}$ increases, $\widehat{h}/\widehat{H}$ increases (figure 11*a*) and $g'/(\Delta/\rho\widehat{H})$ increases (figure 11*b*). As $B/\widehat{H}(\Delta/\rho)^{3/2}$ increases the interface is displaced further from the plume origin and Q increases. The theoretical model (§ 2) shows that as B increases, the product $g'(H-h)$ must increase in order to drive a larger volume flow rate through the space. As the depth $(H-h)$ of the driving layer decreases with B, the upper-layer reduced gravity g' must, therefore, increase. Once a displacement flow was established it was maintained for any further increase in B. However, by reducing B, and thereby increasing $\widehat{F}$, it was possible to revert to a mixing mode of ventilation.

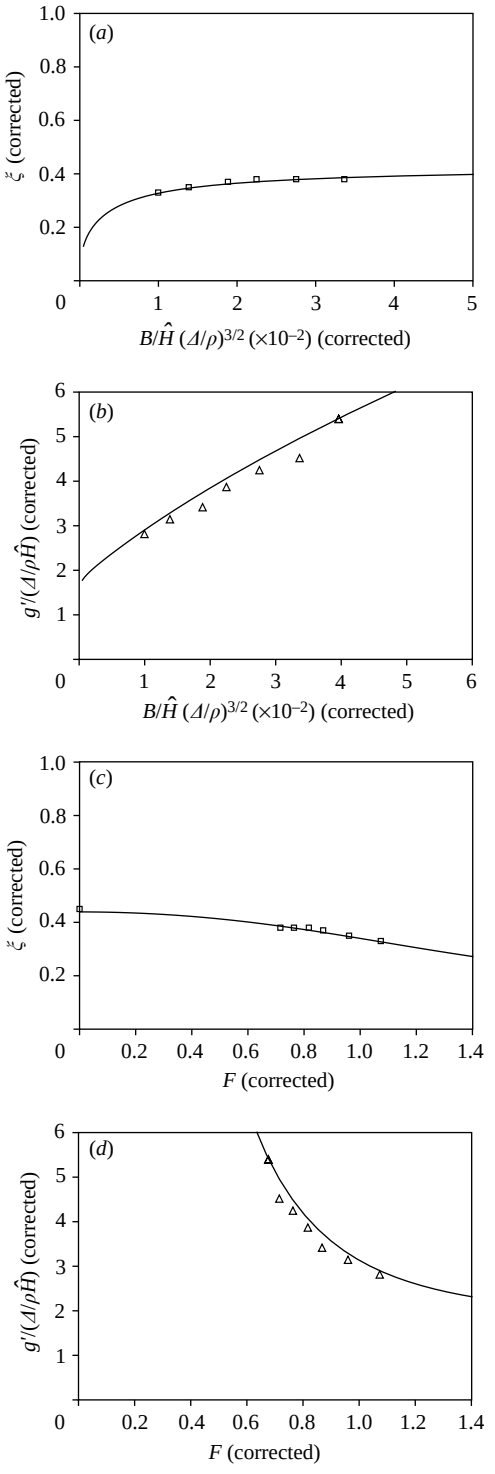

FIGURE 11. Displacement flow – effect of source strength. (*a*) $\xi = \widehat{h}/\widehat{H}$ and (*b*) $g'/(\Delta/\rho\widehat{H})$ plotted against $B/\widehat{H}(\Delta/\rho)^{3/2}$. In (*c*) and (*d*) the same quantities are plotted against $\widehat{F}$. The quantities used in the experiments shown gave $A^*/\widehat{H}^2 = 1.23 \times 10^{-2}$. Predictions from (2.12) and deduced from (2.13) are shown by the continuous curves.

4.2. *Mixing ventilation*

The steady displacement flows described in § 4.1, with two-layer stratification and inflow through leeward openings and outflow through windward openings, were observed to break down for sufficiently large F and a reversed flow through the enclosure was established. An increase in the opposing ventilation flow produced a net loss of buoyancy from the space, and so this reversed flow increased until the stratification was mixed. The buoyancy continued to decrease and the ventilation flow increased until the flux leaving the space equalled that of the source, and a new steady state was established, with a well-mixed interior and a reversed ventilation flow. Results of experiments examining mixing flows are now presented.

4.2.1. *Effect of wind speed*

The mean flow speed in the flume and, hence, Δ (and F) was increased in steps and the average reduced gravity g' of the interior was measured once a steady flow was established. All other quantities were kept constant. The transient stages of the flow leading from a typical steady displacement flow (figure 12*a*, see p. 42) to a steady mixing flow driven by the opposing forces of wind and buoyancy (figure 12*d*) are depicted in figures 12(*b*) and 12(*c*). Figure 12 illustrates the typical transients observed for a significant increase in wind speed. As U_{wind} increased, ambient fluid entered through windward openings. Initially, ambient fluid (figure 12*b*) and, subsequently, buoyant fluid (figure 12*c*) was lost through leeward openings. For a range of U_{wind} the in-flowing fluid rose as a buoyant plume, which collided and mixed with the descending dense plume from the source. The lower saline layer thereby increased in depth and for $F > F_c$ the interface rose until it reached the top of the box. Buoyant fluid then drained through leeward openings and the average density of the fluid in the box decreased with time until a steady mixing flow was established. At higher wind speeds the high momentum of the incoming fluid created an overturning motion within the box and destroyed the stratification before the interface reached the top of the box. Despite these differences in detail, which depend on the geometry of the enclosure and the change in the magnitude of the wind speed, the transition to mixing depends only on whether there is a net loss of buoyancy from the space.

Since the interior is well mixed, results from the mixing ventilation are determined by G' and F – see (2.19), (2.20) and (2.21). Measurements of the steady reduced gravity as a function of F are shown in figure 13 for two different values of A^*/H^2 (as square and triangular symbols), and for a range of other values of opening area (star symbols) and buoyancy flux (circular symbols). As expected the data collapse with the scaling given in § 2.4. We observe that as F increases G' decreases thus implying an increase in Q – see (2.19). Although Q was not measured the reduction in the steady dye concentration within the box (evident through significant colour changes) with increasing Δ gave a qualitative indication of an increasing flow rate.

4.2.2. *Effect of opening area*

In these experiments the wind and buoyancy source were activated simultaneously (giving a constant $Fr = 7.9$), and the effect of first decreasing and then increasing the opening area examined. Initially, all windward and leeward vents were opened and a steady mixing flow was established. After a steady state was reached, the number of openings on both windward and leeward sides was successively reduced by one; dimensionless opening areas considered were $A^*/H^2 = 1.95 \times 10^{-2}$, 1.56×10^{-2}, 1.17×10^{-2}, 7.79×10^{-3}, and 3.90×10^{-3}; these values result in $F = \{2.13, 1.97, 1.79, 1.57, 1.24\}$. A mixing flow was maintained until the final reduction in A^*/H^2 (i.e. as

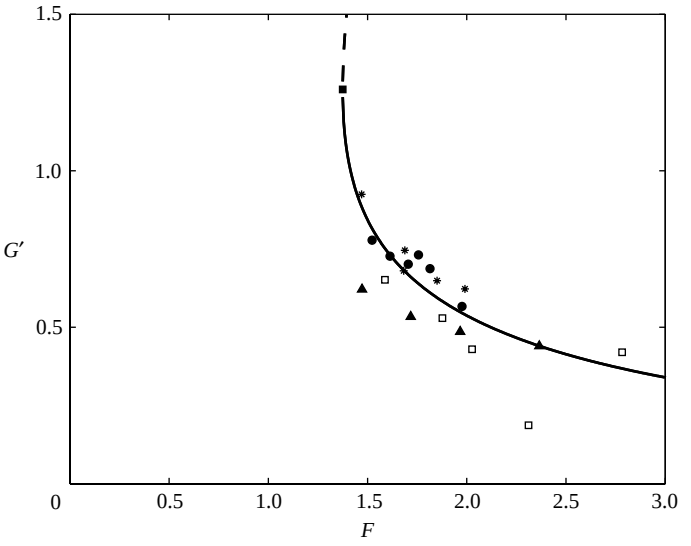

FIGURE 13. Mixing flow. Square symbols: Δ varied with all other quantities fixed, $A^*/H^2 = 2.05 \times 10^{-2}$. Triangular symbols: Δ varied with all other quantities fixed, $A^*/H^2 = 1.23 \times 10^{-2}$. Star symbols: A^* varied with all other quantities fixed. Circular symbols: B varied with all other quantities fixed.

F was reduced from 1.57 to 1.24) which resulted in a displacement flow as expected (see (2.25)). Thus, the direction of the flow is not only dependent on Fr (§ 4.1.1 and § 4.1.2) but also on A^*/H^2. Measurements made with a densitometer, and shown as the star symbols in figure 13, indicate that the reduced gravity increases as the effective opening area (and hence F) decreases.

For the largest opening area considered a counter-clockwise circulation was established in the interior by the inflowing jet. The circulation significantly deflected the plume, although its structure remained clearly visible. As A^*/H^2 was reduced the flow pattern in the interior changed qualitatively from a re-circulating cell to interacting plumes; a dense plume descending from the source and forced buoyant plumes rising from the inlets. In the steady state the region outside the plume appeared well mixed and this was confirmed by measurement. On decreasing the opening area to $A^*/H^2 = 3.90 \times 10^{-3}$ the direction of the flow through the box reversed, and an interface slowly formed at the top of the box and gradually descended until a two-layer stratification was visible with an interface at $h/H \approx 0.15$ and a lower-layer reduced gravity of $g'/G'_H \approx 13$.

On increasing A^*/H^2 from 3.90×10^{-3} to 7.79×10^{-3}, displacement flow was maintained and little change observed in the interface position with $h/H \approx 0.16$ and $g'/G'_H \approx 12$. The difference in internal temperatures between the mixing and displacement flows is dramatic with the mixing flow producing an interior approximately 70% cooler than the displacement flow. This result once more confirms the importance of the time history of these flows. On increasing the opening area the interface rose slowly, and a mixing flow was established and maintained.

4.2.3. *Effect of buoyancy flux*

The effect of the variation of B is also shown in figure 13 (circular symbols). Mixing flows were maintained for a range of $B/H(\Delta/\rho)^{3/2}$ and the reduced gravity g'

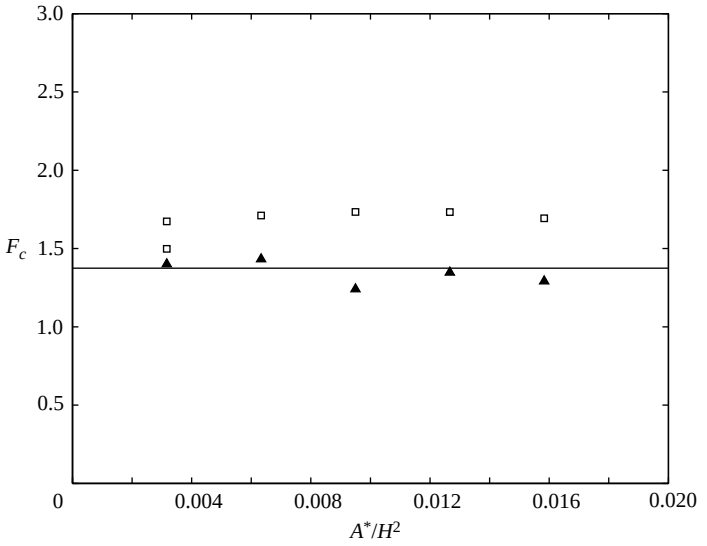

FIGURE 14. F_c plotted against A^*/H^2. Square symbols – displacement to mixing flow (increasing U_{wind}), triangular symbols – mixing to displacement flow (decreasing U_{wind}). The results shown were obtained for small incremental changes in U_{wind}. The straight line gives the critical value $F_c = 1.3747$ from (2.25) for the transition from mixing to displacement ventilation.

increased with increasing $B/H(\Delta/\rho)^{3/2}$, thus implying a decrease in the volume flow rate. Measurements indicate an approximately linear increase in g' with $B/H(\Delta/\rho)^{3/2}$.

The quantitative differences between the experimental points and the theoretical estimate may result from errors in determining Δ or be a result of incomplete mixing within the space in the mixing ventilation.

By further increasing the buoyancy flux it was possible to reduce F below the critical value. When this occurred an interface slowly formed at the top of the box, there was a reversal in the flow direction, and the flow pattern changed from a mixing to a displacement mode of ventilation.

4.3. *Hysteresis*

The theory presented in § 2 predicts two distinct steady flows for identical conditions of wind speed and heat gains within an enclosure when wind opposes the buoyancy-driven flow. The two flows are qualitatively different: either displacement ventilation occurs, with strong stratification and flow out through the upper openings, or mixing ventilation occurs, with a mixed interior and flow in through the upper openings. The flow realized for a given set of conditions is dependent on the time history of the flow as confirmed by experiment.

In order to investigate further the hysteresis in the system the critical value F_c, which marks the transition from displacement to mixing ventilation, was determined for a range of values of A^*/H^2. For a given opening area, a purely buoyancy-driven displacement flow was first established and then U_{wind} was gradually increased until it was just strong enough to establish a steady mixing flow. The wind speed U_{wind} was then increased further before being gradually reduced until a displacement flow was re-established. The critical value F_c, determined in this manner, is shown as a function of A^*/H^2 in figure 14 where it is apparent that $F_c \approx 1.4$ and is independent of A^*/H^2.

The transition from displacement to mixing flow (square symbols) occurs at a higher value of F than the transition from mixing to displacement flow (triangular symbols).

The critical F (denoted by squares on figure 14) defining a transition from displacement to mixing flow was determined by incrementing the wind speed sufficiently gradually that buoyant fluid was not lost through the leeward openings during the transients (at least while the steady interface heights remained below the upper openings). As a result of the gradual increase in wind speed, the total buoyancy within the space was at a maximum immediately prior to transition to mixing. Thus, the value of F immediately before transition represents the maximum F possible while maintaining displacement flow (for the given enclosure and opening geometry).

If the wind speed was increased in larger increments, from any subcritical initial wind speed, such that buoyant fluid was lost during this transient phase, it was possible to bring about transition with a smaller wind speed than that which gives F_c. In other words, it was possible to 'jump' or bypass the critical conditions and set up mixing flow. Determining the total wind speed (or change in wind speed) necessary to bring about transition from displacement to mixing flow when beginning from an arbitrary initial value of F was not practical, particularly given the broad range of incremental changes in wind speed that could be considered. The values of F_c shown in figure 14, however, may be regarded as approximate lower (triangles) and upper (squares) bounds on the wind speed.

5. Conclusions

The effect of an opposing wind on the steady thermal stratification and flow rate developed by a point source of buoyancy in a naturally ventilated enclosure with upper and lower openings has been examined. We have developed theoretical models to describe the steady-state flows that show close agreement with measurements from laboratory experiments in which saline plumes were used to generate buoyancy forces and a flume was used to generate an opposing wind.

Buoyancy-driven flows opposed by wind are characterized by the relative strengths of the wind-induced and buoyancy-induced velocities within the enclosure described by the parameter F defined by (2.8), and the dimensionless area A^*/H^2 of the ventilation openings.

For weak winds (small F), buoyancy dominates and a stable two-layer stratification and displacement flow is established and maintained. Increases in wind speed reduce the ventilation flow rate and increase the depth and temperature of the buoyant upper layer. Qualitatively, the same effects are achieved by decreasing the dimensionless opening area. At high wind speeds (large F) the wind-induced flow dominates and prevents the formation of a stratified interior and mixing ventilation occurs. Outside the plume the interior is well mixed and increases in wind increase the ventilation rate and reduce the internal temperature. Increasing the dimensionless opening area also increases the ventilation rate.

At intermediate wind speeds, one of two stable flows, either a displacement flow or mixing flow, is possible. These flows have fundamentally different properties. The displacement flow has a stratified interior and a smaller ventilation rate than the mixing flow in which the interior has an approximately uniform temperature. If heat removal at low ventilation rates is required, displacement ventilation is more efficient, since the temperature of the air leaving the space is greater than in mixing ventilation. A third, unstable mixing flow is also predicted. The time history of the flow plays an important role in determining which of the steady flows is observed. For a given

enclosure geometry, the transition from a mixing to a stratified displacement flow occurs at a unique value of the Froude number F_c. Higher wind speeds are necessary to maintain mixing flows as the opening area decreases.

In contrast, the reverse transition from displacement to mixing flow occurs for $F > F_c$ due to the additional energy needed to break down the stratification (see Appendix C). Qualitative differences were observed in the transient behaviour depending on the magnitude of the change in wind speed. For gradual increments in wind speed displacement flows can be maintained for higher F than for large incremental changes.

The form of the stratification and rate of ventilation depends not only on F and A^*/H^2 but also on the time history of the flow. For example, if the flow is purely wind-driven initially and at a later stage buoyancy is supplied, the turbulent flow induced by the wind may prevent the plume from establishing stratification within the space. Alternatively, if a stratification is initially established and the building is then exposed to wind, the buoyancy-driven flow may remain dominant and the general two-layer stratification may be maintained.

Although the present experiments are restricted to a simple room geometry and opening locations the results have general application to transitions between mixing and displacement ventilation. Quantitative differences will occur for spaces with different aspect ratios and openings not directly on the windward and leeward façades. Openings at other heights may produce different internal flows and transient effects, but the behaviour we discuss should be robust since it is their elevation with respect to the neutral pressure level that determines whether they act as inflow or outflow vents.

The authors would like to thank the Building Research Establishment for their financial support through the Department of the Environment's Energy Related Environmental Issues (EnREI) in Buildings programme. We are grateful to Brian Dean, David Page-Croft, David Lipman and Caspar Williams for technical assistance. We are also grateful for the comments of a referee who helped clarify the role of the velocities within the space.

Appendix A. Mixing flow – buoyant source supplying mass

Denoting the steady volume flux of fluid expelled through the leeward openings as Q^L, the steady volume flux entering through windward openings as Q^W, and the (constant) volume flux supplied by the source as Q_s, by conservation of volume we require

$$Q^W + Q_s = Q^L. \tag{A 1}$$

When the steady state is reached the mass flux entering the enclosure is identical to the mass flux expelled and, hence, by conservation of mass

$$Q^W \rho + Q_s \rho_s = Q^L \rho_b, \tag{A 2}$$

where ρ, ρ_s and ρ_b denote the density of the ambient fluid, the density of the fluid supplied by the buoyant source and the average density in the enclosure, respectively. If we assume that Q_s is small compared with Q^W, then applying conservation of momentum over a control volume containing the windward and leeward openings, using the neutral pressure level and conservation of volume yields

$$\frac{Q^W}{A^*(BH/A^*)^{1/3}} = (F^2 - G_b')^{1/2} \tag{A 3}$$

where G'_b is defined as

$$G'_b = \frac{g'_b A^{*2/3} H^{1/3}}{B^{2/3}} \tag{A 4}$$

and

$$g'_b = g\frac{\rho - \rho_b}{\rho}. \tag{A 5}$$

Combining (A 1) and (A 2) gives the steady reduced gravity g'_b in the space, namely,

$$\frac{g'_b}{g'_s} = \frac{Q_s}{Q^W + Q_s}, \tag{A 6}$$

where g'_s denotes the initial reduced gravity of the source and is defined as

$$g'_s = g\frac{\rho - \rho_s}{\rho}. \tag{A 7}$$

For a pure heat source $Q_s \equiv 0$.

Appendix B. Calculations for a building

Steady-state predictions of interface height, upper-layer temperature and air flow rate in a building 10 m tall which is naturally ventilated by the opposing forces of wind and buoyancy are shown in table 1. For comparative purposes the example considered here is based on the example given in HL in which the wind assisted the buoyancy. The distance between the centre of the upper opening and the ceiling is 1 m. The top of the lower opening is 1 m above the floor, and the vertical distance between the midpoints of the upper and lower openings is 8 m. The effective area of the openings has been chosen to produce an interface at a height of 5 m above the floor when the flow is driven solely by a point source of buoyancy of strength 0.5 kW. Predictions of h, T_u (upper-layer temperature), Q and the air changes per hour ACH are given in the first column of table 1 for buoyancy-driven flows; the remaining three columns show predictions for the buoyancy-driven flow opposed by a wind of speed 1, 2 and 4 m s^{-1}, respectively. The mixing flow is assumed to be established once the steady-state interface height falls below the level of the lower opening.

Appendix C. Transition between displacement and mixing flows

At high wind speeds the wind-driven flow may be strong enough to destroy a stable stratification and generate a mixed interior. The exact mechanism by which this occurs is complicated and depends on the form and strength of the stratification, the geometry of the space and the change in wind speed. To obtain a global estimate of the required flow rates to induce a mixing flow we use the concept of mixing efficiency (Linden 1979).

Broadly speaking turbulence is an inefficient mixer as the majority of the turbulence kinetic energy is dissipated by viscosity and only a small fraction (around 20%) of the turbulence energy is used to mix the stratification thereby increasing the potential energy. Consider a space with a two-layer stratification and interface at height h above the floor with a reduced gravity g' across the interface. The increase in potential energy when this stratification is completely mixed is

$$\Delta PE = \tfrac{1}{2}\rho g' h(H - h)S, \tag{C 1}$$

	Buoyancy	Buoyancy opposed by wind		
U_{wind} (m s^{-1})	0	1	2	4
Fr	0	6	12	24
A^* (m^2)	1.495	1.495	1.495	1.495
F	0	1.48	2.96	5.91
h (m)	0.50	2.76	1.38	–
Flow class	Displace.	Displace.	Displace.	Mixing
T_a (°C)	15.0	15.0	15.0	15.0
T_u (°C)	15.8	17.1	21.8	15.1
Q (m^3 s^{-1})	4.98	0.19	0.06	3.98
ACH	17.9	0.7	0.2	14.3

TABLE 1. A comparison between steady-state natural ventilation flows driven by buoyancy forces alone and those opposed by wind. The source strength is 0.5 kW and the pressure coefficients at the windward inlet and leeward outlet are taken to be $C_{pi} = 0.7$ and $C_{po} = -0.2$, respectively. The physical properties of the ambient air at 15°C are taken to be $\beta = 3.48 \times 10^{-3}\,\mathrm{K}^{-1}$, $C_P = 1012\,\mathrm{J kg}^{-1}\,\mathrm{K}^{-1}$ and $\rho = 1.225\,\mathrm{kg\,m}^{-3}$, see Batchelor (1967), p. 594. The number of air changes per hour (ACH) is based on an enclosure of volume $V = 1000\,\mathrm{m}^3$. T_a denotes the temperature of the ambient.

where S is the cross-sectional floor area (assumed constant). The volume of inflow required to lower the interface to the floor (assuming the inflowing fluid is confined to within the buoyant layer) is hS and, hence, the kinetic energy added over this time (i.e. $t = hS/Q$) is

$$\Delta KE = \frac{\rho S H Q^2}{2A^{*2}}, \tag{C 2}$$

where, for simplicity, we have assumed the inflow rate Q is constant. The mixing efficiency is then

$$\eta = \frac{\Delta PE}{\Delta KE} = \frac{g'h(H-h)A^{*2}}{Q^2 H}. \tag{C 3}$$

If there is inflow through windward vents $Q = A^*(\Delta/\rho - g'(H-h))^{1/2}$ and, hence, from (C3) we obtain

$$\eta = \frac{h}{H}\left(\frac{1}{\widetilde{F}^2} - 1\right), \tag{C 4}$$

where

$$\widetilde{F} = \sqrt{\frac{\Delta}{\rho g'(H-h)}}. \tag{C 5}$$

Expressing (C4) in terms of the wind pressure drop we have

$$\frac{\Delta}{\rho} = \left[\left(\frac{h}{H}\right)\frac{1}{\eta} + 1\right] g'(H-h). \tag{C 6}$$

In other words, the wind-induced velocity must be a factor of $[(h/H)/\eta + 1]^{1/2}$ greater than the buoyancy-induced velocity to establish a mixing flow. For an interface at half height and taking $\eta = 0.2$ (which is a generous estimate) the wind must increase the buoyancy flow rate by almost a factor of two. Such large inflows of wind-driven ventilation are usually not permitted because of discomfort to the occupants. This

analysis shows that the interior stratification plays a dominant role in determining the flow patterns within the space even on windy days.

REFERENCES

Batchelor, G. K. 1967 *An Introduction to Fluid Dynamics*. Cambridge University Press.

Hunt, G. R. & Holford, J. M. 2000 The discharge coefficient – experimental measurement of a dependence on density contrast. *Proc. 21st AIVC Conference, The Hague, Netherlands*. 12pp.

Hunt, G. R & Kaye, N. G. 2001 Virtual origin correction for lazy turbulent plumes. *J. Fluid Mech.* **435**, 377–396.

Hunt, G. R. & Linden, P. F. 1997 Laboratory modelling of natural ventilation flows driven by the combined forces of buoyancy and wind. *Proc. CIBSE National Conf., October 1997*, Vol. 1, pp. 101–107.

Hunt, G. R. & Linden, P. F. 1998 Time-dependent displacement ventilation caused by variations in internal heat gains: application to a lecture theatre. *Proc. Roomvent '98, the 6th International Conference on Air Distribution in Rooms*, *Stockholm, Sweden*, Vol. 2, pp. 203–210.

Hunt, G. R. & Linden, P. F. 1999 The fluid mechanics of natural ventilation – displacement ventilation by buoyancy-driven flows assisted by wind. *Building & Environment* **34**, 707–720.

Hunt, G. R. & Linden, P. F. 2000 Multiple steady airflows and hysteresis when wind opposes buoyancy. *Air Infiltration Rev*. **21**, 1–3.

Hunt, G. R. & Linden, P. F. 2001 Steady-state flows in an enclosure ventilated by buoyancy forces assisted by wind. *J. Fluid Mech.* **426**, 355–386 (referred to herein as HL).

Kaye, N. B. & Hunt, G. R. 2004 Time dependent flows in an emptying filling box. *J. Fluid Mech.* **520**, 135–156.

Li, Y. & Delsante, A. 2001 Natural ventilation induced by combined wind and thermal forces. *Building & Environment* **36**, 59–71.

Linden, P. F. 1979 Mixing in stratified fluids. *Geophys. Astrophys. Fluid Dyn.* **13**, 3–23.

Linden, P. F. 2000 Convection in the environment. In *Perspectives in Fluid Mechanics*. (ed. G. K. Batchelor, H. K. Moffatt & M. G. Worster.), pp. 289–345. Cambridge University Press.

Linden, P. F., Lane-Serff, G. F. & Smeed, D. A. 1990 Emptying filling boxes: the fluid mechanics of natural ventilation. *J. Fluid Mech.* **212**, 300–335.

Morton, B. R., Taylor, G. I. & Turner, J. S. 1956 Turbulent gravitational convection from maintained and instantaneous sources. *Proc. R. Soc. Lond.* A **234**, 1–23.

Turner, J. S. 1986 Turbulent entrainment: the development of the entrainment assumption, and its application to geophysical flows. *J. Fluid Mech.* **173**, 431–471.